GEOCHEMISTRY

Fe-oxide concretions formed by interacting carbonate and acidic waters on Earth and Mars

H. Yoshida[1*†], H. Hasegawa[1,2*†], N. Katsuta[3], I. Maruyama[4], S. Sirono[4], M. Minami[5], Y. Asahara[4], S. Nishimoto[6], Y. Yamaguchi[4], N. Ichinnorov[7], R. Metcalfe[8]

Spherical Fe-oxide concretions on Earth, especially in Utah, USA, have been investigated as an analog of hematite spherules found in Meridiani Planum on Mars to support interpretations of water-rock interactions in early Mars. Although several formation mechanisms have been proposed for the Fe-oxide concretions on Earth, it is still unclear whether these mechanisms are viable because a precise formation process and precursor of the concretions are missing. This paper presents evidence that Fe-oxide concretions in Utah and newly found Fe-oxide concretions in Mongolia had spherical calcite concretions as precursors. Different formation stages of calcite and Fe-oxide concretions observed, both in Utah and Mongolia, indicate that calcite concretions initially formed within eolian sandstone strata and were dissolved by infiltrating Fe-rich acidic waters to form spherical FeO(OH) crusts due to pH buffering. The similarity between these Fe-oxide concretions on Earth and the hematite spherule occurrences in Meridiani Planum, combined with evidence of acid sulfate water influences on Mars, suggest that the hematite spherules also formed from dissolution of preexisting carbonate spherules possibly formed under a dense carbon dioxide early martian atmosphere.

INTRODUCTION

Fe-oxide concretions in the Jurassic Navajo Sandstone of southern Utah, USA have been studied as analogs of hematite spherules (known as blueberries) found by NASA's Opportunity rover in Meridiani Planum on Mars (Fig. 1) (*1*–*11*). A debate lasting nearly two decades has produced several models for the origin of the Fe-oxide concretions in the Navajo Sandstone. However, the precise formation mechanism of the terrestrial Fe-oxide concretions is still uncertain, which limits their value as analogs for martian hematite spherules.

One previous model for the Fe-oxide concretions in Utah suggested that Fe-oxide concretions formed by mixing between reducing fluids and oxygenated water, which caused precipitation of iron as ferric oxide cement in the bleached host rock (*1*, *2*, *4*–*8*). Mobilization and transport of chemically reduced Fe^{2+} in solution are thought to have occurred via groundwater flow with CH_4 or other hydrocarbons as reducing agents (*4*, *6*, *8*). However, this model does not well explain the development of spherical concretions with Fe-rich crusts. The other model proposed microbially mediated decomposition of preexisting spherical siderite concretions as a formation mechanism for Fe-rich crusts (*9*–*11*). Although there are microscopic pseudomorph-like textures, which have been interpreted as being originally siderite crystals (*11*), these occur within the interiors of some Fe-oxide concretions. However, firm evidence for preexisting concretions consisting entirely of siderite has never been found. In addition, the precipitation of precursor siderite in the highly porous eolian sandstone strata (*9*) is questionable due to the lack of similar geological evidence.

Here, we propose a new model for the formation of Fe-oxide concretions based on field evidence that preexisting calcite concretions were precursors of Fe-oxide concretions at two localities: the Jurassic Navajo Sandstone, Utah, and the Cretaceous Djadokhta Formation, Mongolia (Fig. 1, A and B, and Table 1). In this new model, Fe-oxide concretions formed due to pH buffering as preexisting calcite concretions dissolved in infiltrating Fe-rich acidic waters, leading to fixation of Fe as FeO(OH) crusts. This new model can be applied to commonly observed Fe-oxide concretions and/or crusts (e.g., pipe-like textures) at other sites that formed in similar sedimentary facies and environmental conditions. On the basis of this evidence, we reassess the value of the terrestrial concretions as analogs for the hematite spherules observed in Meridiani Planum on Mars (Fig. 1C) (*1*–*3*, *12*).

RESULTS

Field observation of concretions in Utah and Mongolia

The Lower Jurassic Navajo Sandstone, which is widely distributed in Utah, is composed of fine- to medium-grained eolian sandstone with a variety of colors due to variations in its bleaching state (*4*, *5*, *8*, *9*, *11*). In general, whitish "bleached" sandstone occurs in the upper part of the formation, whereas reddish "unbleached" sandstone is present in the lower part. Fe-oxide concretions occur dominantly in the upper part just above a bleaching front. On the other hand, spherical calcite concretions occur within the lower reddish unbleached sandstone in the east of Escalante (Spencer Flat) and north of Kanab (White Cliff) (*5*). These calcite concretions have similar sizes and morphologies to the Fe-oxide concretions within the upper whitish bleached sandstone (Fig. 1A and figs. S1 and S2). At Spencer Flat, partly dissolved calcite concretions stained by Fe-oxide crusts are also present just below the bleaching front. Occurrences of calcite concretions and partly dissolved calcite concretions stained by Fe-oxide crusts within the unbleached reddish sandstone were also reported in previous studies (*5*, *8*). These studies suggested that the upper part of the Navajo Sandstone was originally red and was bleached by hydrocarbon-rich or organic acid-rich fluids (*4*, *5*, *8*, *9*, *11*). Intensive bleaching, interpreted to have been caused by CO_2-charged acidic fluids, was also observed in drilled cores of the upper part of the Navajo Sandstone as well as in permeable eolian strata and along faults and fractures (*13*, *14*).

[1]Material Research Section, Nagoya University, University Museum, Nagoya, Japan. [2]Faculty of Science and Technology, Kochi University, Kochi, Japan. [3]Faculty of Education, Gifu University, Gifu, Japan. [4]Graduate School of Environmental Studies, Nagoya University, Nagoya, Japan. [5]Institute for Space-Earth Environmental Research, Nagoya University, Nagoya, Japan. [6]Nagoya City Science Museum, Nagoya, Japan. [7]Institute of Paleontology and Geology, Mongolian Academy of Science, Mongolia. [8]Quintessa Limited, The Hub, Henley-on-Thames, Oxfordshire, UK.
*These authors contributed equally to this work.
†Corresponding author. Email: dora@num.nagoya-u.ac.jp (H.Y.); hito_hase@kochi-u.ac.jp (H.H.)

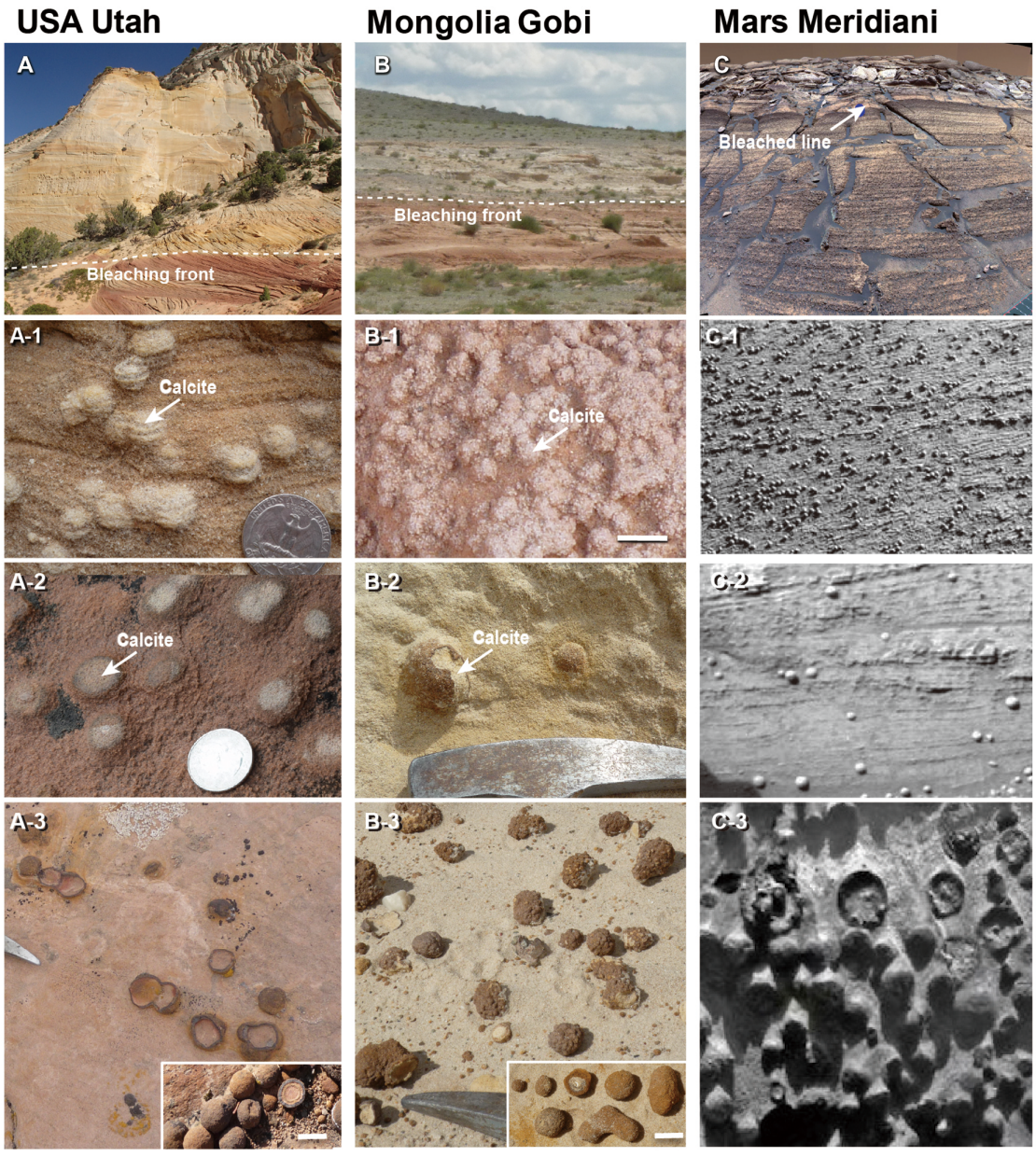

Fig. 1. Similarity of concretions on Earth (Utah and Mongolia) and Mars (Meridiani Planum). Occurrences of calcite concretions and Fe-oxide concretions in the Jurassic Navajo Sandstone of Spencer Flat in Grand Staircase–Escalante National Monument (GSENM; 37°40′15″N, 111°23′0″W) and White Cliff (37°12′45″N, 112°23′24″W), Utah (**A**) and in the Cretaceous Djadohta Formation of the Tugrikiin Shiree area, southern Mongolia (44°13′54″N, 103°16′33″E) (**B**). These concretions are compared with similar concretions from the Meridiani Planum on Mars (**C**). In the localities on Earth, calcite concretions are preserved below bleaching fronts (A-1 and B-1; stage 1). Fe-oxide concretions formed during bleaching, and typically calcite is preserved inside (arrow; A-2 and B-2; stage 2), surrounded by a hard Fe-rich crust (A-3 and B-3; stage 3). Hematite spherules on Mars have similar occurrences and morphologies [C-1 and C-2: hematite spherules "blueberries" in Burns formation at Eagle crater, Meridiani Planum (image from the Opportunity sol 123 and sol 42) (*3*, *25*); C-3: spherules with Fe-oxide crust texture "newberries" in Matijevic formation at Endeavour crater, Meridiani Planum (image from the Opportunity sol 3064) (*12*)]. Scale bars, 1 cm. All photos of Utah and Mongolia are taken by H. Yoshida.

Spherical calcite concretions and Fe-oxide–encrusted calcite concretions also occur in the Upper Cretaceous Djadokhta Formation of the Tugrikiin Shiree, southern Mongolia (Fig. 1B and fig. S3) and show similar morphologies to the concretions in Utah. In general, the Djadokhta Formation is reddish colored, but in the Tugrikiin Shiree, it is distinguishable by the occurrence of whitish bleached sandstone (*15*). The area where bleaching is observed near Tugrikiin Shiree is surrounded by Cenozoic volcanic rocks (fig. S3) (*16*, *17*). In contrast, underlying intercalated fluvial sandstone and mudstone strata are characterized by reddish unbleached strata and include aggregates of spherical calcite concretions. The distributions of calcite and Fe-oxide concretions in Mongolia, below and above the bleaching front, are similar to those of Utah.

Mineralogical and geochemical analyses of concretions

X-ray diffraction (XRD) analysis of calcite concretions and the cores of Fe-oxide concretions from both Utah and Mongolia identified calcite in all development stages of the concretions (fig. S4). In contrast, no siderite was identified, either inside the calcite concretions or inside the Fe-oxide concretions. XRD analysis also confirmed that the Fe-oxide crusts are composed mainly of goethite [FeO(OH)] and hematite (Fe_2O_3) (*8*). Optical microscopic observations of the calcite concretions in both Utah and Mongolia show that micritic calcite grew in the micropores of the sandstone matrices (figs. S2, D-3, and S3, C-ii and C-iii) to form spherical calcite concretions that crosscut sedimentary laminae. The textures indicate that the calcite concretions formed during early diagenesis and grew in situ authigenically.

The calcite concretions from both Utah and Mongolia show $\delta^{13}C$ values of −5.15 to −3.13‰ and −3.50 to −1.65‰, respectively (Table 2). The calcite cements in the surrounding matrices of both host rocks have slightly lower values of −7.44 to −3.36‰ (Utah) and −8.21 to −3.79‰ (Mongolia). On the other hand, the values of $\delta^{18}O$ of the calcite concretions are −12.0 to −5.06‰ (Utah) and ~ −11.8 to −10.1‰ (Mongolia) (Table 2). The $\delta^{13}C$ and $\delta^{18}O$ data imply that the concretions from both areas formed under similar conditions and that, in each area, the source of the carbon in the carbonate minerals was mainly meteoric water that penetrated from the ground surface (*18*, *19*).

Elemental mapping by secondary x-ray analytical microscopy (SXAM) reveals the replacement stages of the calcite concretions by FeO(OH) that thickened inward from the surfaces of preexisting calcite concretions (Fig. 2 and figs. S5 and S6). In stage 1, concretions from both Utah and Mongolia have almost homogeneous calcite distributions (Fig. 2A, stage 1) and concentrations of 15 to 25 weight % (wt %) $CaCO_3$ measured by x-ray fluorescence (XRF) analysis (Table 2). In these concretions, the space occupied by the calcite is almost the same as the original porosity of the Navajo Sandstone and Djadokhta Formation (c. 20 volume %) (*6*). In the intermediate stage 2 of both Utah and Mongolia examples, $CaCO_3$ concentrations decrease from the insides of concretions toward their outer surfaces (Fig. 2, B and C). In contrast, Fe concentrations gradually increase close to the surfaces of the concretions within Fe-oxide crusts (Fig. 2, B and C). Fe-oxide crusts then become thicker, growing inward, and the volume of remaining $CaCO_3$ is reduced in stage 3 (Fig. 2D). The peaks of the Fe profiles develop close to the surfaces of the calcite concretions and correspond to depletions in the $CaCO_3$ contents of the concretions. These observations indicate that Fe was fixed to form Fe-oxide crusts as the Fe-rich acidic water diffused inward during pH buffering by calcite cement dissolution on the surfaces of concretions (*20*). The Fe-oxide concretions therefore grew inward from the surfaces of the original calcite concretions. The acidic water also contained Mn that precipitated on the outsides of the Fe-oxide crusts, producing a consistent correlation between Fe and Mn concentrations (Fig. 2 and figs. S5 and S6) (*21*).

A similar Fe profile was also produced by experiments simulating the pH-buffering reaction during bleaching of the surrounding reddish sandstone and dissolution of preexisting calcite concretions (fig. S7). We carried out experiments using spherical calcite concretions collected from within eolian sand in Utah and an acid, Fe-rich solution $FeCl_2$ (pH = 3 to 4). During experiments, Fe-oxide crusts

Table 1. Comparison of previous models (① and ②) and our proposed model (③).

	Formation mechanism	Precusor	Reaction fluid/liquid	Fe-oxide mineralization	Fe state
① Chan *et al.* model	Goethite precipitation by redox-oxic reaction	None	Buoyant, reducing fluid due to hydrocarbon	Precipitation of goethite (not clear for crust formation)	Fe^{2+}
② Loope *et al.* model	Siderite formation and microbial oxidation	Siderite (not found)	Reducing groundwater with methane dissolved	Internal Fe source (siderite)	Fe^{2+}
③ Our proposed model	Calcite-acid reaction by pH buffering	Calcite (found)	Penetration of CO_2-charged acidic groundwater	Inward precipitation of goethite by Fe-rich acidic water from outside	Fe^{3+}

Table 2. Carbon contents, $\delta^{13}C_{VPDB}$, $\delta^{18}O_{VPDB}$ (CF-IRMS), and $CaCO_3$ concentrations (XRF and estimated volume) of calcite concretions (stages 1 and 2) and host rock sandstone from Utah and Mongolia. VPDB, Vienna Pee Dee Belemnite; CF-IRMS, continuous flow isotope ratio mass spectrometry.

	Location and samples	C (wt %)	$CaCO_3$ (wt %)	$\delta^{13}C_{VPDB}$ (‰)	$\delta^{18}O_{VPDB}$ (‰)
Utah (USA)	Ca concretion (Escalante)	3.46–4.48	15.0–15.7	−5.15 to −3.13	−10.1 to −5.06
	Host rock sandstone	0.01–0.51	0.13–0.14	−5.96 to −3.36	−10.3 to −8.56
	Ca concretion (White Cliff)	1.80–2.63	15.0–21.9*	−4.63 to −4.21	−12.0 to −11.5
	Host rock sandstone	0.01<	0.03–0.08*	−7.44 to −6.81	−12.9 to −2.02
Gobi (Mongolia)	Ca concretion	3.85–6.29	18.8–24.4	−3.50 to −1.65	−11.5 to −10.1
	Host rock sandstone	0.01–1.12	0.01*–0.56	−8.21 to −3.79	−11.8 to −11.2

*Estimated volume.

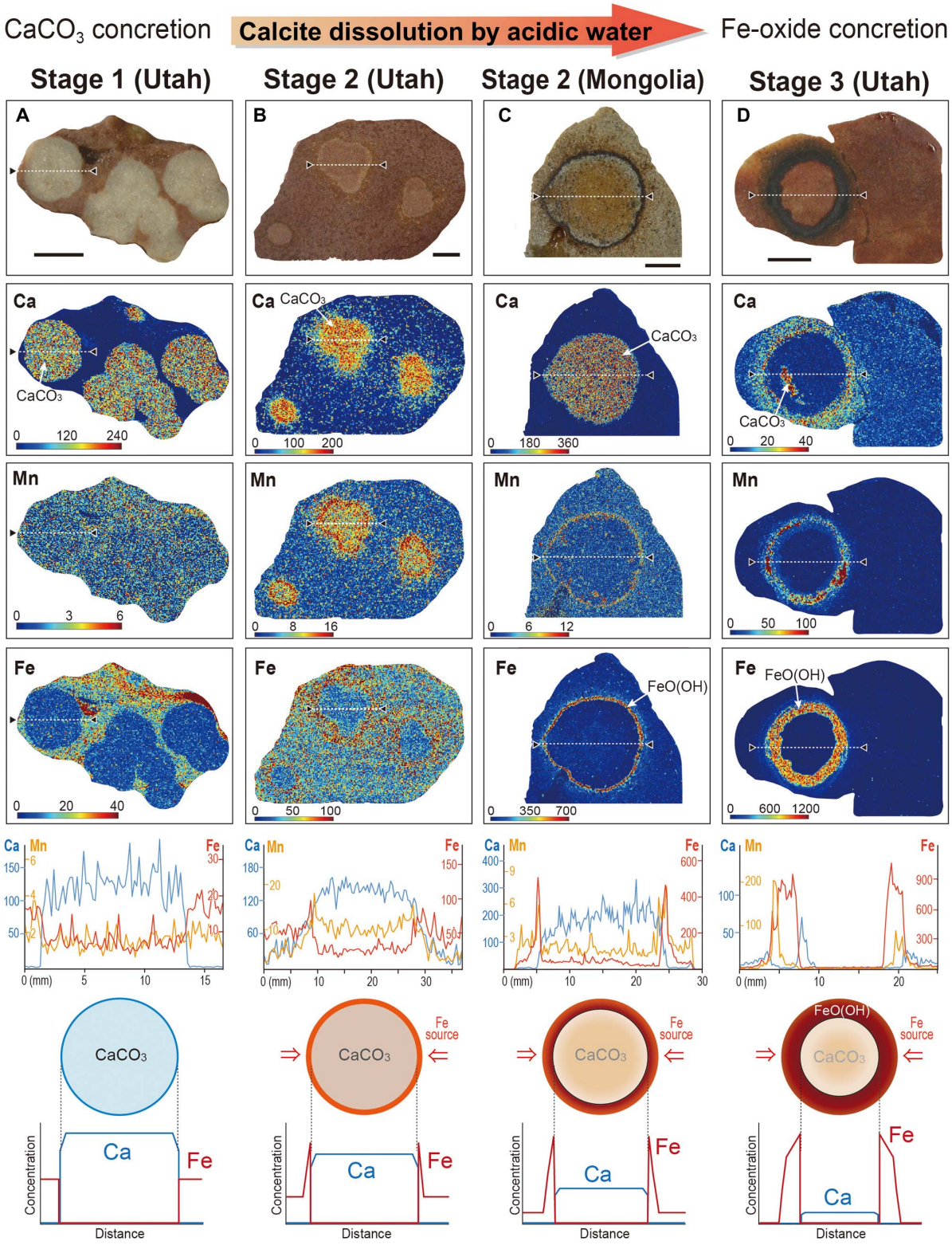

Fig. 2. Elemental mapping of different development stages of concretions in Utah and Mongolia. SXAM profiles across buried calcite and Fe-oxide concretions from Utah and Mongolia show the different stages (stages 1 to 3) of concretion formation due to interaction between ferric iron mobilized in acidic water and precursor calcite concretions. Stage 1: Spherical calcite concretions formed in eolian sandstone. Stage 2: Start of Fe-rich crust formation by reaction with calcite in Utah and in Mongolia. Stage 3: Almost all the calcite has been dissolved out, and a thick Fe-oxide crust has developed around a "ghost" spherical calcite concretion. An Fe profile across an Fe-rich crust, developed around a calcite concretion, shows a high Fe peak at the reaction front on the concretion surface. This observation indicates that acidic water provided Fe from outside the concretion rather than the Fe being sourced inside the concretion. Scale bars, 1 cm.

formed on the surfaces of the calcite concretion after only 2 months. Although the compositions of the experimental solution and natural water from which the concretions formed probably differed, the experiment illustrates the viability of the proposed concretion formation mechanism. The features of an experimentally produced Fe-oxide crust, including the higher Fe peak concentration profile close to the calcite concretion surface, are similar to those of the natural Fe-oxide concretions observed in both Utah and Mongolia (Fig. 2 and figs. S5 and S6).

DISCUSSION

Formation model for Fe-oxide concretions

On the basis of the above field, geochemical and experimental evidence, we propose the following mechanism for Fe-oxide concretion formation (Fig. 3): (i) Spherical calcite concretions initially formed in calcite-saturated groundwater within the eolian sandstone strata during early diagenesis; (ii) subsequently, the calcite concretions were dissolved by penetration of Fe-rich acidic waters; and (iii) mobilized Fe in acidic waters was fixed to form FeO(OH) (goethite) crusts on the preexisting spherical calcite concretion surfaces due to the pH-buffering reaction. A similar Fe-rich crust profile on a calcite concretion surface was also replicated by a simple pH-buffering experiment (fig. S7).

Differences between previously proposed models of Fe-oxide concretion formation and the new model are summarized in Table 1 and by the following chemical reactions (Eqs. 1 to 6). The first model is a "redox-oxic reaction model" (*1*, *2*, *4*–*8*) in which Fe-oxide concretions can precipitate via oxidation of ferrous iron in solution according to Eq. 1

$$2Fe^{2+} + 0.5O_2 + 3H_2O = 2FeO(OH)(\text{goethite}) + 4H^+ \quad (1)$$

This model requires ferrous iron to be released from minerals and transported in solution via groundwater, possibly with the required reducing conditions being produced by CH_4 or other hydrocarbons (*4*, *8*) or possibly by reduced sulfur species such as H_2S (*4*). However, this model cannot fully explain why spherical Fe-oxide–encrusted concretions were formed.

The second model is the "siderite formation and microbial oxidation model" (*9*–*11*), which can be summarized by an oxidation reaction in Eq. 2

$$4FeCO_3 + O_2 + 10H_2O = 4Fe(OH)_3 + 4HCO_3^- + 4H^+ \quad (2)$$

In this model, a spherical siderite concretion is both an Fe source and a precursor of a spherical Fe-oxide–encrusted concretion. The siderite concretion undergoes oxidative dissolution, which is possibly microbially mediated and which provides an internal source of Fe that forms an Fe-oxide crust on the outside the concretion. However, a problem with this model is that no siderite concretions have been identified, neither in outcrop (*6*, *8*, *9*) nor in any deeper environment at these localities (*13*). In addition, all detailed observations on sections through the Fe-oxide concretions (*8*), including the elemental mapping analysis (Fig. 2 and figs. S5 and S6), and the results of calcite dissolution and pH-buffering experiments (fig. S7) indicate that Fe must be provided from outside a concretion. The peaks of the Fe profiles develop close to the surfaces of the remaining calcite. Even if the siderite concretions previously existed, an internal source of Fe by siderite dissolution cannot explain the Fe profiles. Furthermore, $\delta^{13}C$ values of calcite remaining inside Fe-oxide concretions (Table 2) are inconsistent with an organic source (*9*–*11*).

In contrast to these previous models, we propose a new model, whereby the Fe-oxide concretions form by pH-buffering reactions between Fe-rich acidic water and calcite concretions (Eqs. 3 to 6 and Fig. 3) (*22*–*24*). First, spherical calcite concretions precipitated in calcite-saturated groundwater within the buried eolian sandstone strata during early diagenesis (Eq. 3). Initially, microsized calcite crystals formed as nuclei, and then subsequent concretion growth proceeded throughout the interconnected pore spaces, leading to the in situ formation of larger, isolated spherical authigenic concretions. The spherical geometry is the minimum free-energy shape that forms in nature

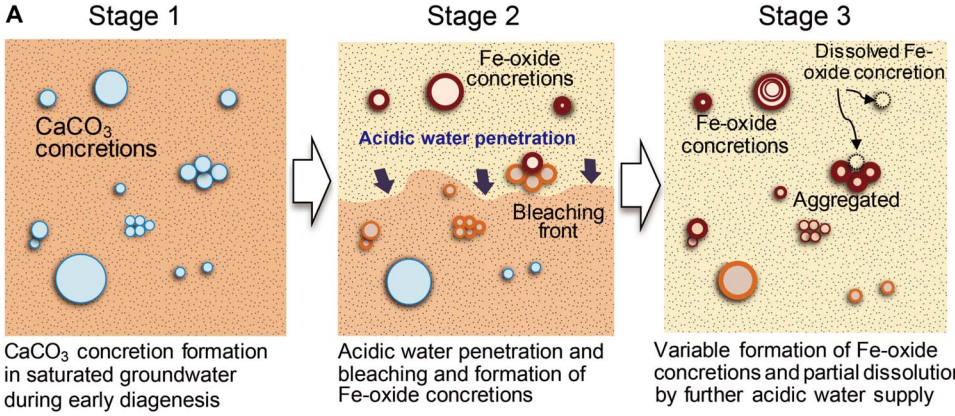

Fig. 3. Formation process of Fe-oxide concretions on Earth. Generalized model for the formation of Fe-oxide concretions by acid water penetration through the eolian sandstone strata and subsequent reaction with spherical calcite concretions. Stage 1: Different sizes and shapes of calcite concretion were formed from calcite-saturated groundwater within buried eolian sandstone deposits during early diagenesis. Stage 2: Episodic acidic water penetration and formation of Fe-oxide concretion by pH buffering by calcite dissolution. The CO_2-charged acidic groundwater flowed laterally under the influence of gravity, leading to its localized and heterogeneous bleaching. Stage 3: Variable shapes of Fe-oxide concretions that reflect the shapes of the precursor calcite concretions until the calcite has been completely dissolved. Subsequently, some of the Fe-oxide concretions could be dissolved by later acidic water penetration.

where the host rock is relatively homogeneous (*1*). As a result, similarly sized calcite concretions formed in the local area

$$Ca^{2+} + 2HCO_3^- = CaCO_3 + H_2O + CO_2 \quad (3)$$

Subsequently, acidic water (pH < 3 to 4) dissolves hematite from eolian sandstone (iron grain coatings) to mobilize ferric iron, thereby bleaching the reddish-colored sandstone (Eq. 4). Then, the acidic water dissolves the surface of a calcite concretion (Eq. 5). According to this reaction, the dissolution of a calcite concretion consumes H^+, thereby increasing pH and causing the mobilized ferric iron to precipitate as goethite on the concretion surface (Eq. 6). Namely, fixation of Fe-oxide crusts occurred because of a pH-buffering reaction as Fe-rich acidic water dissolved the calcite cement on concretion surfaces. This Fe-rich water diffused into the concretions, leading to replacement of the calcite from outside the concretions inward

$$Fe_2O_3 + 6H^+ = 2Fe^{3+} + 3H_2O \quad (4)$$

$$CaCO_3 + 2H^+ = Ca^{2+} + H_2O + CO_2 \quad (5)$$

$$Fe^{3+} + 2H_2O = FeO(OH) + 3H^+ \quad (6)$$

Unlike the two earlier models, our model does not involve either the reducing fluids produced by groundwater reacting with CH_4 or other hydrocarbons (*1*, *2*, *4*–*8*) or siderite formation and microbial mediation process (*9*–*11*). In addition, the model does not require reduced fluids to mix with oxic water at the location of concretion formation. Instead, in our new model, there is only a simple pH-buffering reaction between spherical calcite concretions and penetration of acidic groundwater. The profiles of the Fe concentration peaks formed during crust development are quite consistent with the process that Fe was provided by a solution originating from outside the concretion rather than from inside (Fig. 2 and figs. S5 to S7). Liesegang-type Fe-oxide concretion formation, as commonly observed in the Navajo Sandstone (*6*–*8*), also supports the interpretation that the Fe source was infiltrating acid water (fig. S6). The occurrences at the reaction fronts of bands with the highest Fe concentrations indicate that Fe was supplied only from outside the concretions rather than originating inside the cores of the concretions (*20*, *25*).

In Utah, the groundwater could have acquired its acidity from CO_2 either generated from natural reservoirs that are widely developed in the Colorado Plateau (*13*) or provided directly by magmatic sources (*26*). Extensive volcanic activity of middle-late Cenozoic age in this area could have possibly liberated CO_2 to the groundwater (fig. S1). In this case, the resulting CO_2-charged acidic groundwater led to hematite dissolution in the reddish eolian sandstone strata, thereby bleaching it. The CO_2-charged acidic groundwater could have flowed laterally along permeable sedimentary units under the influence of gravity (*13*, *14*). These processes can explain occurrences of heterogeneous bleaching structures (*5*, *7*) and locally extended streak-like "tails" (*9*). Similarly, acidic waters in Mongolia could have possibly originated in a volcanic field near Tugrikiin Shiree (fig. S3) during the Oligocene (c. 35 to 30 million years) (*16*, *17*). In both Utah and Mongolia, the acidic groundwater mobilized Fe from the eolian reddish sandstone, rather extensively in Utah and relatively localized in Mongolia. The spatial distributions of bleached strata and Fe-oxide concretions indicate the influence area of acidic waters (Fig. 4).

Some studies also report the presence of calcite within bleached strata in Utah (*5*), which seems to be inconsistent with the proposed model. However, as shown in Eq. 4, the acidic water first dissolves hematite from eolian sandstone to mobilize ferric iron, thereby bleaching the reddish-colored sandstone and increasing the water's pH. In addition, acidic water would be neutralized by dissolution of aluminosilicate minerals present in the sandstone. On the basis of these multibleaching and pH-buffering processes, calcite concretions in the strata may not be always have completely dissolved in the bleached strata.

After the precipitation of goethite, the pore space of the sandstone was filled, which would have decreased the diffusion coefficient of the sandstone and caused the migration rate of the reaction front to decrease (*27*). We performed simple numerical simulations of $CaCO_3$ dissolution and Fe^{3+} precipitation to estimate formation time scales of Fe-oxide concretions (see the Supplementary Materials). The activities of ions (H^+ and Fe^{3+}) are set to be varied in ranges between $10^{-2} < H^+ < 10^{-1}$ and $10^{-3} < Fe^{3+} < 10^{-1}$, respectively. We solved diffusion equations for both ions including precipitation of Fe^{3+} and dissolution of $CaCO_3$. Precipitation of Fe^{3+} proceeds at the surfaces of $CaCO_3$ concretions. The simulation results indicate that the time scale for formation of an Fe-oxide crust of millimeter-scale thickness is on the order of 1 to 10 years if the flux of acidic water is negligible and concentrations of the ions are constant at large distances from the concretions. The reactions probably continued until the pore space had been sealed or the calcite in a concretion had been almost completely dissolved. If acidic water penetration and reaction had continued after the calcite concretions had completely dissolved, then goethite would also have been dissolved and been removed thereafter (Fig. 3). We also estimated the time scale for bleaching (Fe_2O_3 dissolution) of eolian reddish sandstone strata (see the Supplementary Materials). On the basis of piezometric pressure gradients ranging from ~10^4 to 4 × 10^6 Pa/m (*28*), a solute concentration of 10^{-5} M, and a permeability of 10^{-14} m^2, a time scale on the order of 10^5 to 10^7 years might be necessary to bleach a rock thickness of 200 m in the upper part of the Navajo Sandstone, within which the Fe-oxide concretions formed.

The previously published lower Fe isotopic values of Fe-oxide concretions (*29*, *30*) can also be explained by the proposed model. Iron oxide concretions have slightly lower $\delta^{56}Fe$ (~ −1.5‰) compared with Fe oxides in the matrix of the Navajo Sandstone (~ +0.3‰). In the previous study, the difference of Fe isotope values was explained by reduction of Fe in the iron oxide source and some subsequent oxidation. However, this fractionation of iron isotopes between the matrix and concretions can also be explained by kinetic isotope fractionation during the migration and precipitation of the dissolved ferric iron (*31*).

In summary, a schematic model for Fe-oxide concretion formation in the studied strata of Utah and Mongolia is summarized in Fig. 4. First, after burial of the eolian sandstone deposits, calcite concretions were formed from calcite-saturated groundwater during early diagenesis in the Jurassic (Utah) and Cretaceous (Mongolia). Subsequently, the CO_2-charged acidic groundwater dissolved hematite in the reddish eolian sandstone to mobilize Fe, thereby bleaching the reddish sandstone during the Cenozoic. When the acidic groundwater encountered the calcite concretions, the calcite concretions were dissolved. Mobilized Fe precipitated on the preexisting calcite concretion surfaces due to the increased pH, thereby producing outer rinds

consisting of Fe oxyhydroxide. The reactions involved in forming the Fe-oxyhydroxide–encrusted concretions probably continued until the pore space had been sealed or the calcite in a concretion had been almost completely dissolved. If the reactions ceased before complete dissolution of a calcite concretion, then Fe-oxyhydroxide–encrusted calcite was preserved. When this Fe-oxyhydroxide–encrusted calcite was exposed at the surface by erosion, any remaining calcite was dissolved, and Fe-oxide–encrusted concretions were preserved. This explains why many of the Fe-oxide–encrusted concretions are observed near the bleached front today (Fig. 4). If acidic water penetration and reaction had continued after the calcite concretions had completely dissolved, then goethite would also have dissolved and been removed. The spatial distribution of the rind-type Fe-oxide concretions therefore reflects the area of acidic water penetration (Fig. 4).

Analogy with martian hematite spherule

We propose that a similar formation process can explain the formation of hematite spherules in Meridiani Planum on Mars (Figs. 1C and 4) (*1*–*3*, *12*, *32*, *33*). The upper part of the sedimentary sequences in Meridiani Planum are rich in hematite, and hydrated sulfate minerals including jarosite (*3*, *24*, *32*–*35*), which are thought to be diagnostic of formation from acidic (pH ~ 3 to 5) and oxidizing, Fe-rich surface waters, and/or a fluctuating groundwater table (*24*, *33*, *36*–*38*). These low-pH sulfate waters are thought to have originated from sulfur gas released from degassing of the Tharsis volcano (*36*) and/or evaporation of surface waters (*37*) during the Hesperian period [c. 3.7 to 3.2 billion years (Ga)]. Remote sensing analysis also confirms that the Meridiani Planam is located where there are higher concentrations of hydrous Fe sulfate (*39*). Evidence for acid sulfate water influences and the occurrence of hematite spherules in Meridiani Planum suggest the possibility that the formation mechanism of martian spherules could have been similar to that of the Fe-oxide concretions in Utah and Mongolia on Earth.

In the Meridiani Planum, hematite spherules (blueberries) were abundantly identified in the lower part of the Burns formation exposed around the Eagle and Endurance craters (*3*, *32*, *33*), which shows downward infiltration of acidic water (*33*, *35*). The upper part of the formation around Erebus crater, which does not include obvious spherules, shows a stronger influence of acidic water infiltration. Some of the hematite spherules in the lower part of the formation have crusts, a so-called "rind and overgrowth texture" (*7*, *35*), which are similar to the Fe-oxyhydroxide crusts of the Utah and Monglian concretions. This similarity suggests that, similar to these terrestrial Fe-oxyhydroxide crusts, the martian hematite crusts can be explained

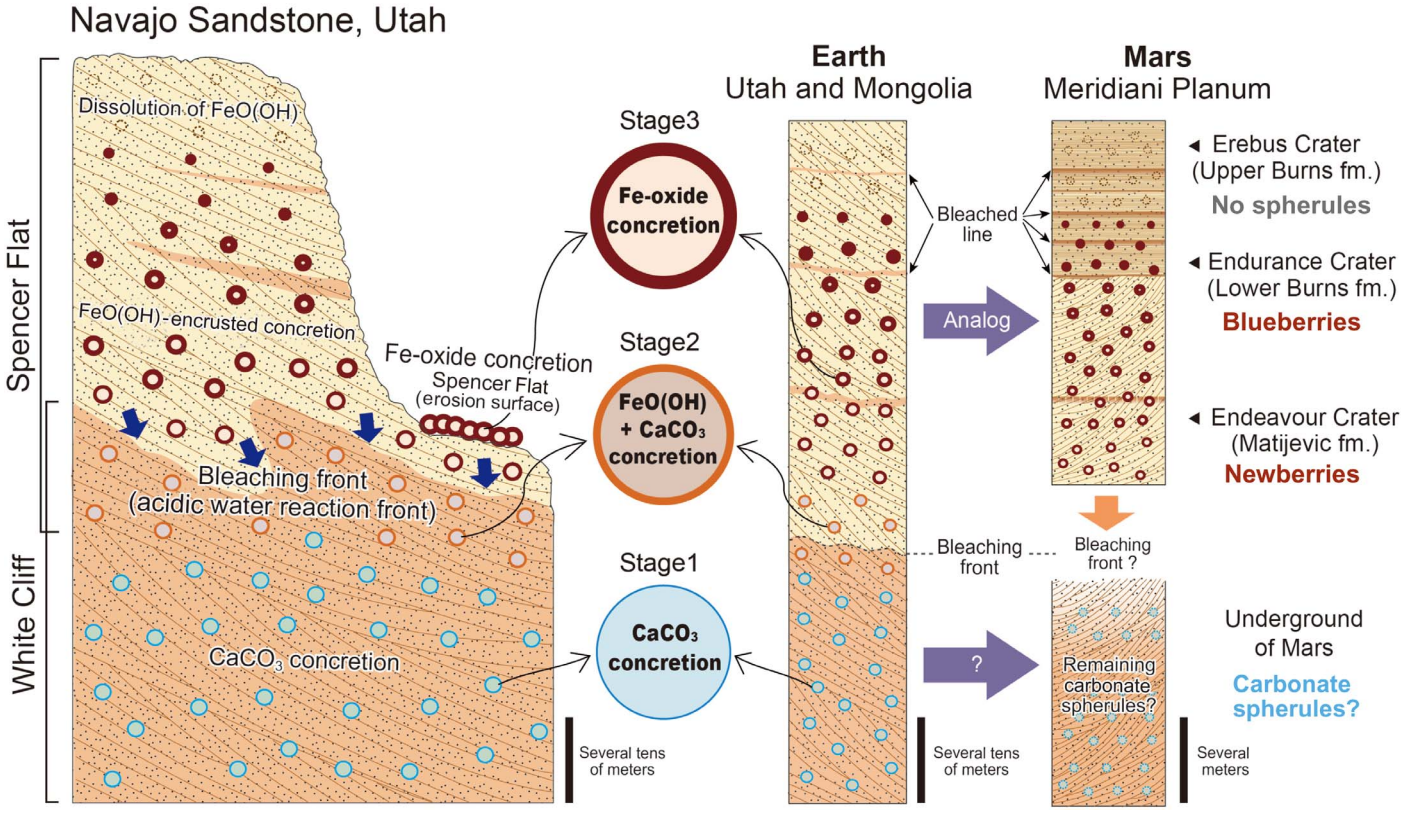

Fig. 4. Schematic illustration of Fe-oxide concretion formation on Earth and Mars. Fe-oxide concretion formation from spherical calcite concretion precursors during pH-buffering reactions that are interpreted to have occurred across the bleaching fronts observed in Utah and Mongolia and across an assumed bleaching front on Mars. The spatial distributions of Fe-oxide concretions at different stages of formation (e.g., rinds) and dissolution are considered to reflect the penetration of Fe-rich acidic waters. Acidic waters dissolved hematite in the reddish eolian sandstone to mobilize Fe, thereby bleaching the reddish-colored sandstone. When the acidic water encountered the calcite concretions, the calcite concretions were dissolved. At the same time, mobilized Fe precipitated on the preexisting calcite concretion surface due to the increased pH, thereby producing outer rinds consisting of Fe oxyhydroxide. When Fe-oxyhydroxide–encrusted calcite concretions were exposed, any remaining calcite dissolved. In the uppermost part of the succession, Fe-oxide concretions dissolved completely. Right column shows a model for the distributions of hematite spherules and expected relict carbonate spherules in underground strata at Meridiani Planum, Mars.

by pH buffering on the surfaces of preexisting carbonate spherules. In addition, recently found spherules in the stratigraphically lower Matijevic formation around the Botany Bay area at Meridiani Planum have much clearer rind structures (newberries) (*12*, *40*, *41*). Presumably, these spherules formed where there was less influence of acid sulfate water (*12*, *33*), suggesting that a bleaching front caused by the infiltrated acidic water may exist at around this horizon (Fig. 4). Increased FeO/MnO ratios in the spherule-rich area analyzed by the alpha particle x-ray spectrometer of the Opportunity rover (*12*) can also be interpreted as evidence for changing pH conditions at the reaction front between the Fe oxide and preexisting carbonate spherules. These observations are similar to the observed variations in Fe and Mn concentrations across the Fe-oxide concretions from Utah and Mongolia (Fig. 2 and figs. S5 and S6).

On the basis of this evidence, we propose that hematite spherules in Meridiani Planum were possibly formed by interaction between preexisting carbonate spherules and acid sulfate water that infiltrated early in martian history. Our model can reasonably accept the classical hypothesis that widespread carbonate deposition occurred in the late Noachian (c. 3.8 to 3.7 Ga), and that the carbonate then dissolved again in the Hesperian period (c. 3.7 to 3.2 Ga) (*24*, *33*, *36*, *38*). Our model also requires an oxidizing surface environment on early Mars, which is consistent with the recent finding of Mn-oxide occurrences in the Meridiani Planum (*42*).

Although the studied terrestrial concretions have some features that are analogous to those of the martian spherules, the sizes of the martian hematite spherules are notably smaller (mean size, c. 3 to 5 mm) than those of the Fe-oxide concretions (mean size, c. 20 to 30 mm with various size range) on Earth (*1*, *3*, *7*). The size differences could be attributed to formation conditions of precursor carbonate concretion/spherule on Earth and Mars, that is, (i) diffusion coefficient, (ii) solute concentration, and (iii) CO_2 solubility. These factors are also related to temperatures, evaporation rates, and atmospheric pressures that prevailed on Earth and Mars. First, the diffusion coefficient of sandstone strata, containing both terrestrial concretions and martian spherules, is thought to be similar (both strata are well sorted with similar grain sizes) (*3*, *32*). Then, according to Fairén *et al.* (*43*), higher evaporation rates resulted in increasing solute concentrations in martian groundwater. These conditions promoted formation of the martian spherules. On the other hand, the expected lower groundwater temperature on Mars could have caused lower solute concentration in association with decreased chemical weathering. In addition, the cooler martian conditions also prevented the precipitation of carbonate by increasing the solubility of CO_2 in groundwater (Eq. 3). We therefore consider that the small size of the martian spherules is possibly caused by the lower solute concentration and increased CO_2 solubility due to the lower groundwater temperature on Mars.

Implication for early martian history

Compared to the present, the martian atmosphere before 3.8 Ga (before the late Noachian) was undoubtedly denser, and the climate was warmer and wetter (*36*, *44*, *45*). Carbonate minerals have been invoked as a possible sink for the CO_2 in the denser early Mars atmosphere. However, distributions of carbonate occurrences on the present-day martian surface are limited (*46*–*48*). The cause of the missing carbonates can be explained by our model, that is, dissolution of preexisting carbonate across the martian surface during the Hesperian period (*36*, *46*). The abundant hematite spherules in Meridiani Planum can therefore be considered as relicts of precursor carbonate and evidence of a primordial CO_2-rich atmosphere on early Mars.

Contrary to the above interpretation, a recent model using mineral and contextual sedimentary environmental data obtained by NASA's Curiosity rover suggests a circum-neutral pH for pore waters in lacustrine sediments of the Sheepbed member of the Gale crater and casts doubt on a denser early Mars atmosphere (*49*). On the other hand, subsequent data from the Curiosity rover suggest moderate to alkaline conditions for the Sheepbed member and acidic conditions for the overlying Murray formation (*50*, *51*), implying that strata of Gale crater may have undergone a complex alteration history. This also suggests the possibility that pore water conditions of the Sheepbed member could have changed from an initial alkaline condition to a neutral condition due to the influence of acidic water. Therefore, it is still plausible that initial carbonate deposition under a relatively dense CO_2 atmosphere was followed by carbonate dissolution under acidic conditions early in martian history. Ancient Mars apparently hosted aqueous environments in a variety of alteration settings in which waters ranged widely from acidic to alkaline (*36*, *38*, *50*). It is necessary to understand such diverse alteration conditions and the history of water-mineral interaction in each region to assess the past and present habitability of Mars.

MATERIALS AND METHODS

Geological surveys were carried out to investigate the Navajo Sandstone at Spencer Flat, east of Escalante, Utah, at White Cliff north of Kanab, Utah (figs. S1 and S2), and the Djadokhta Formation in the Tugrikiin Shiree in southern Mongolia (fig. S3). The purpose was to find in situ calcite concretions that could be precursors of Fe-oxide concretions. Buried Fe-oxide concretions were sampled to analyze Ca (or $CaCO_3$) that might remain in the cores of concretions with Fe-rich rinds.

Mineralogical characterization [thin section, scanning electron microscopy with energy-dispersive spectroscopy (SEM-EDS) and XRD] and geochemical analyses (XRF) of concretions and surrounding rock matrices were conducted in the Nagoya University Museum and Graduate School of Environmental Science of Nagoya University. Mineralogical compositions were determined with an XRD (Multiflex, Rigaku Co.) using crushed and powered samples and Cu Kα radiation (the Cu being subjected to an electron beam of 40 kV/20 mA). XRD patterns show clear differences between the calcite contents of the concretions and surrounding matrix (fig. S4).

A secondary SXAM method using an XRF analyzer (XGT-2000V, HORIBA, Japan) to show semiquantitatively the two-dimensional distribution of elements Fe, Mn, and in particular Ca across the whole surface of a sample was used at the Department of Education, Gifu University, Gifu, Japan (Fig. 2 and figs. S5 to S7). A high-intensity continuous x-ray beam (Rh anode, 50 kV/1 mA), 100 μm in diameter, is focused with a guide tube and irradiated perpendicular to the surface of the sample, which is located on a PC-controllable *X*-*Y* stage. XRF from the sample surface is analyzed with the hp-Si detector of an EDS.

The carbon and oxygen isotopes of calcite concretions were measured by a CF-IRMS with a gas chromatography system (DELTA V Plus with GasBench, Thermo Fisher Scientific Inc.) at Shoko Scientific Co. Ltd. Each sample was placed in a septum-sealed vial filled with He gas and then reacted with H_3PO_4 introduced using a syringe. After being reacted, the evolved CO_2 gas was carried into a CF-IRMS in a He carrier gas to measure the $\delta^{13}C_{VPDB}$ and $\delta^{18}O_{VPDB}$, which

were conventionally represented with respect to VPDB (Table 2). Their errors are ±0.1‰ and ±0.1‰ (1σ), respectively.

SUPPLEMENTARY MATERIALS

Supplementary material for this article is available at http://advances.sciencemag.org/cgi/content/full/4/12/eaau0872/DC1

Section S1. Geological setting
Section S2. Mineralogical and geochemical analysis of concretions
Section S3. Experimental formation of Fe-oxide concretions
Section S4. Numerical simulation to estimate formation time scales
Fig. S1. Landsat image, geologic map, CO_2 reservoir and volcanic rock distribution, and conceptual model of CO_2-charged groundwater in Utah.
Fig. S2. Outcrop photographs, morphologies and microscopic textures of Fe-oxide, and calcite concretions in Utah.
Fig. S3. Location map, outcrop photographs, morphologies and microscopic textures of Fe-oxide, and calcite concretions in Mongolia.
Fig. S4. XRD pattern of concretions and Fe-oxide crusts.
Fig. S5. Elemental distributions in and around the Fe-oxide concretions (stage 2) in Mongolia.
Fig. S6. Elemental distributions in and around the Fe-oxide concretions (stages 2 and 3) in Utah.
Fig. S7. Experimental study of Fe-oxide concretion formation.

REFERENCES AND NOTES

1. M. A. Chan, B. Beitler, W. T. Parry, J. Ormö, G. Komatsu, A possible terrestrial analogue for haematite concretions on Mars. *Nature* **429**, 731–734 (2004).
2. J. Ormö, G. Komatsu, M. A. Chan, B. Beitler, W. T. Parry, Geological features indicative of processes related to the hematite formation in Meridiani Planum and Aram Chaos, Mars: A comparison with diagenetic hematite deposits in southern Utah, USA. *Icarus* **171**, 295–316 (2004).
3. S. W. Squyres, J. P. Grotzinger, R. E. Arvidson, J. F. Bell III, W. Calvin, P. R. Christensen, B. C. Clark, J. A. Crisp, W. H. Farrand, K. E. Herkenhoff, J. R. Johnson, G. Klingelhöfer, A. H. Knoll, S. M. McLennan, H. Y. McSween Jr., R. V. Morris, J. W. Rice Jr., R. Rieder, L. A. Soderblom, In situ evidence for an ancient aqueous environment at Meridiani Planum, Mars. *Science* **306**, 1709–1714 (2004).
4. B. Beitler, M. A. Chan, W. T. Parry, Bleaching of Jurassic Navajo Sandstone on Colorado Plateau Laramide highs: Evidence of exhumed hydrocarbon supergiants? *Geology* **31**, 1041–1044 (2003).
5. B. Beitler, W. T. Parry, M. A. Chan, Fingerprints of fluid flow: Chemical diagenetic history of the Jurassic Navajo Sandstone, southern Utah, U.S.A. *J. Sediment. Res.* **75**, 547–561 (2005).
6. W. T. Parry, Composition, nucleation, and growth of iron oxide concretions. *Sediment. Geol.* **233**, 53–68 (2011).
7. S. L. Potter, M. A. Chan, E. U. Petersen, M. D. Dyar, E. Sklute, Characterization of Navajo Sandstone concretion: Mars comparison and criteria for distinguishing diagenetic origins. *Earth Planet. Sci. Lett.* **301**, 444–456 (2011).
8. M. A. Chan, S. L. Potter, B. B. Bowen, W. T. Parry, L. M. Barge, W. Seiler, E. U. Petersen, J. R. Bowman, Characteristics of terrestrial ferric oxide concretions and implications for Mars, in *Sedimentary Geology of Mars* (SEPM Special Publication, 2012), pp. 253–270.
9. D. B. Loope, R. M. Kettler, K. A. Weber, Follow the water: Connecting a CO_2 reservoir and bleached sandstone to iron-rich concretions in the Navajo Sandstone of south-central Utah. U.S.A. *Geology* **38**, 999–1002 (2010).
10. K. A. Weber, T. L. Spanbauer, D. Wacey, M. R. Kilburn, D. B. Loope, R. M. Kettler, Biosignatures link microorganisms to iron mineralization in a paleoaquifer. *Geology* **40**, 747–750 (2012).
11. D. B. Loope, R. M. Kettler, The footprints of ancient CO_2-driven flow systems: Ferrous carbonate concretions below bleached sandstone. *Geosphere* **11**, 943–957 (2015).
12. R. E. Arvidson, S. W. Squyres, J. F. Bell III, J. G. Catalano, B. C. Clark, L. S. Crumpler, P. A. de Souza Jr., A. G. Fairén, W. H. Farrand, V. K. Fox, R. Gellert, A. Ghosh, M. P. Golombek, J. P. Grotzinger, E. A. Guinness, K. E. Herkenhoff, B. L. Jolliff, A. H. Knoll, R. Li, S. M. McLennan, D. W. Ming, D. W. Mittlefehldt, J. M. Moore, R. V. Morris, S. L. Murchie, T. J. Parker, G. Paulsen, J. W. Rice, S. W. Ruff, M. D. Smith, M. J. Wolff, Ancient aqueous environments at Endeavour crater, Mars. *Science* **343**, 1248097 (2014).
13. N. Kampman, M. J. Bickle, A. Maskell, H. J. Chapman, J. P. Evans, G. Purser, Z. Zhou, M. F. Schaller, J. C. Gattacceca, P. Bertier, F. Chen, A. V. Turchyn, N. Assayag, C. Rochelle, C. J. Ballentine, A. Busch, Drilling and sampling a natural CO_2 reservoir: Implications for fluid flow and CO_2-fluid–rock reactions during CO_2 migration through the overburden. *Chem. Geol.* **369**, 51–82 (2014).
14. M. Wigley, N. Kampman, H. J. Chapman, B. Dubacq, M. J. Bickle, In situ redeposition of trace metals mobilized by CO_2-charged brines. *Geochem. Geophys. Geosy.* **14**, 1321–1332 (2013).
15. H. Hasegawa, R. Tada, N. Ichinnorov, C. Minjin, Lithostratigraphy and depositional environments of the Upper Cretaceous Djadokhta Formation, Ulan Nuur basin, southern Mongolia, and its paleoclimatic implication. *J. Asian Earth Sci.* **35**, 13–26 (2009).
16. T. L. Barry, A. D. Saunders, P. D. Kempton, B. F. Windley, M. S. Pringle, D. Dorjnamjaa, S. Saandar, Petrogenesis of Cenozoic basalts from Mongolia: Evidence for the role of asthenospheric versus metasomatized lithospheric mantle sources. *J. Petrology* **44**, 55–91 (2003).
17. V. V. Yarmolyuk, E. A. Kudryashova, A. M. Kozlovsky, V. A. Lebedev, V. M. Savatenkov, Late Mesozoic–Cenozoic intraplate magmatism in Central Asia and its relation with mantle diapirism: Evidence from the South Khangai volcanic region, Mongolia. *J. Asian Earth Sci.* **111**, 604–623 (2015).
18. E. M. E. Khoriby, Origin of calcite-cemented concretions in a fluviatile sequence, the Malha Formation (Lower Cretaceous), El Tih Plateau, East Central Sinai, Egypt. *Mansoura J. Geol. Geophys.* **33**, 91–126 (2006).
19. J. B. Gates, W. M. Edmunds, W. G. Darling, J. Ma, Z. Pang, A. A. Young, Conceptual model of recharge to southeastern Badain Jaran Desert groundwater and lakes from environmental tracers. *Appl. Geochem.* **23**, 3519–3534 (2008).
20. V. Souza-Egipsy, J. Ormö, B. B. Bowen, M. A. Chan, G. Komatsu, Ultrastructural study of iron oxide precipitates: Implications for the search for biosignatures in the Meridiani hematite concretions, Mars. *Astrobiology* **6**, 527–545 (2006).
21. R. J. Barnaby, J. D. Rimstidt, Redox conditions of calcite cementation interpreted from Mn and Fe contents of authigenic calcites. *Geol. Soc. Am. Bull.* **101**, 795–804 (1989).
22. K. B. Krauskopf, D. K. Bird, *Introduction to Geochemistry 3rd Edition* (McGraw-Hill Science, 1994).
23. C. Klein, Some Precambrian banded iron-formations (BIFs) from around the world: Their age, geologic setting, mineralogy, metamorphism, geochemistry, and origins. *Am. Mineral.* **90**, 1473–1499 (2005).
24. A. G. Fairén, D. Fernández-Remolar, J. M. Dohm, V. R. Baker, R. Amils, Inhibition of carbonate synthesis in acidic oceans on early Mars. *Nature* **431**, 423–426 (2004).
25. H. Yoshida, R. Metcalfe, S. Nishimoto, H. Yamamoto, N. Katsuta, Weathering rind formation in buried terrace cobbles during periods of up to 300ka. *Appl. Geochem.* **26**, 1706–1721 (2011).
26. S. M. V. Gilfillan, C. J. Ballentine, G. Holland, D. Blagburn, B. S. Lollar, S. Stevens, M. Schoell, M. Cassidy, The noble gas geochemistry of natural CO_2 gas reservoirs from the Colorado Plateau and Rocky Mountain provinces, USA. *Geochim. Cosmochim. Acta* **72**, 1174–1198 (2008).
27. H. Yoshida, K. Yamamoto, M. Minami, N. Katsuta, S. Sin-ichi, R. Metcalfe, Generalized conditions of spherical carbonate concretion formation around decaying organic matter in early diagenesis. *Sci. Rep.* **8**, 6308 (2018).
28. N. Kampman, A. Busch, P. Bertier, J. Snippe, S. Hangx, V. Pipich, Z. Di, G. Rother, J. F. Harrington, J. P. Evans, A. Maskell, H. J. Chapman, M. J. Bickle, Observational evidence confirms modelling of the long-term integrity of CO_2-reservoir caprocks. *Nat. Commun.* **7**, 12268 (2016).
29. V. Busigny, N. Dauphas, Tracing paleofluid circulations using iron isotopes: A study of hematite and goethite concretions from the Navajo Sandstone (Utah, USA). *Earth Planet. Sci. Lett.* **254**, 272–287 (2007).
30. M. A. Chan, C. M. Johnson, B. L. Beard, J. R. Bowman, W. T. Parry, Iron isotopes constrain the pathways and formation mechanisms of terrestrial oxide concretions: A tool for tracing iron cycling on Mars? *Geosphere* **2**, 324–332 (2006).
31. J. L. Skulan, B. L. Beard, C. M. Johnson, Kinetic and equilibrium Fe isotope fractionation between aqueous Fe(III) and hematite. *Geochim. Cosmochim. Acta* **66**, 2995–3015 (2002).
32. J. P. Grotzinger, R. E. Arvidson, J. F. Bell III, W. Calvin, B. C. Clark, D. A. Fike, M. Golombek, R. Greeley, A. Haldemann, K. E. Herkenhoff, B. L. Jolliff, A. H. Knoll, M. Malin, S. M. McLennan, T. Parker, L. Soderblom, J. N. Sohl-Dickstein, S. W. Squyres, N. J. Tosca, W. A. Watters, Stratigraphy and sedimentology of a dry to wet eolian depositional system, Burns formation, Meridiani Planum, Mars. *Earth Planet. Sci. Lett.* **240**, 11–72 (2005).
33. J. M. Metz, J. P. Grotzinger, D. M. Rubin, K. W. Lewis, S. W. Squyres, J. F. Bell III, Sulphate-rich eolian and wet interdune deposits, Erebus crater, Meridiani Planum, Mars. *J. Sediment. Res.* **79**, 247–264 (2009).
34. M. E. E. Madden, R. J. Bodnar, J. D. Rimstidt, Jarosite as an indicator of water-limited chemical weathering on Mars. *Nature* **431**, 821–823 (2004).
35. S. M. McLennan, J. F. Bell III, W. M. Calvin, P. R. Christensen, B. C. Clark, P. A. De Souza, J. Farmer, W. H. Farrand, D. A. Fike, R. Gellert, A. Ghosh, T. D. Glotch, J. P. Grotzinger, B. Hahn, K. E. Herkenhoff, J. A. Hurowitz, J. R. Johnson, S. S. Johnson, B. Jolliff, G. Klingelhöfer, A. H. Knoll, Z. Learner, M. C. Malin, H. Y. McSween Jr., J. Pocock, S. W. Ruff, L. A. Soderblom, S. W. Squyres, N. J. Tosca, W. A. Watters, M. B. Wyatt, A. Yen, Provenance and diagenesis of the evaporite-bearing Burns formation, Meridiani Planum, Mars. *Earth Planet. Sci. Lett.* **240**, 95–121 (2005).

36. J.-P. Bibring, Y. Langevin, J. F. Mustard, F. Poulet, R. Arvidson, A. Gendrin, B. Gondet, N. Mangold, P. Pinet, F. Forget; the OMEGA team, M. Berthé, J.-P. Bibring, A. Gendrin, C. Gomez, B. Gondet, D. Jouglet, F. Poulet, A. Soufflot, M. Vincendon, M. Combes, P. Drossart, T. Encrenaz, T. Fouchet, R. Merchiorri, G. Belluci, F. Altieri, V. Formisano, F. Capaccioni, P. Cerroni, A. Coradini, S. Fonti, O. Korablev, V. Kottsov, N. Ignatiev, V. Moroz, D. Titov, L. Zasova, D. Loiseau, N. Mangold, P. Pinet, S. Douté, B. Schmitt, C. Sotin, E. Hauber, H. Hoffmann, R. Jaumann, U. Keller, R. Arvidson, J. F. Mustard, T. Duxbury, F. Forget, G. Neukum, Global mineralogical and aqueous Mars history derived from OMEGA/Mars express data. *Science* **312**, 400–404 (2006).
37. J. A. Hurowitz W. W. Fischer, N. J. Tosca, R. E. Milliken, Origin of acidic surface waters and the evolution of atmospheric chemistry on early Mars. *Nat. Geosci.* **3**, 323–326 (2010).
38. B. L. Ehlmann, J. F. Mustard, S. L. Murchie, J.-P. Bibring, A. Meunier, A. A. Fraeman, Y. Langevin, Subsurface water and clay mineral formation during the early history of Mars. *Nature* **479**, 53–60 (2011).
39. S. Karunatillake, J. J. Wray, O. Gasnault, S. M. McLennan, A. D. Rogers, S. W. Squyres, W. V. Boynton, J. R. Skok, L. Ojha, N. Olsen, Sulfates hydrating bulk soil in the Martian low and middle latitudes. *Geophys. Res. Lett.* **41**, 7987–7996 (2014).
40. W. H. Farrand, J. F. Bell, J. R. Johnson, M. S. Rice, B. L. Jolliff, R. E. Arvidson, Observations of rock spectral classes by the Opportunity rover's Pancam on northern Cape York and on Matijevic Hill, Endeavour Crater, Mars. *J. Geophys. Res. Planets* **119**, 2349–2369 (2014).
41. A. G. Fairén, S. W. Squyres, J. P. Grotzinger, W. M. Calvin, S. W. Ruff, Hollowed spherules identified with the MER opportunity near and at Cape York, Western Rim of Endeavour Crater, Mars, Abstract in *45th Lunar and Planetary Science Conference* (Universities Space Research Association, 2014), vol. 45, p.1566.
42. R. E. Arvidson, S. W. Squyres, R. V. Morris, A. H. Knoll, R. Gellert, B. C. Clark, J. G. Catalano, B. L. Jolliff, S. M. McLennan, K. E. Herkenhoff, S. VanBommel, D. W. Mittlefehldt, J. P. Grotzinger, E. A. Guinness, J. R. Johnson, J. F. Bell III, W. H. Farrand, N. Stein, V. K. Fox, M. P. Golombek, M. A. G. Hinkle, W. M. Calvin, P. A. de Souza Jr., High concentrations of manganese and sulfur in deposits on Murray Ridge, Endeavour Crater, Mars. *Am. Mineral.* **101**, 1389–1405 (2016).
43. A. G. Fairén, C. Gil-Lozano, E. R. Uceda, E. Losa-Adams, A. F. Davila, L. Gago-Duport, Mineral paragenesis on Mars: The roles of reactive surface area and diffusion. *J. Geophys. Res. Planets* **122**, 1855–1879 (2017).
44. B. M. Jakosky, R. J. Phillips, Mars' volatile and climate history. *Nature* **412**, 237–244 (2001).
45. R. Hu, D. M. Kass, B. L. Ehlmann, Y. L. Yung, Tracing the fate of carbon and the atmospheric evolution of Mars. *Nat. Commun.* **6**, 10003 (2015).
46. B. L. Ehlmann, J. F. Mustard, S. L. Murchie, F. Poulet, J. L. Bishop, A. J. Brown, W. M. Calvin, R. N. Clark, David J. Des Marais, R. E. Milliken, L. H. Roach, T. L. Roush, G. A. Swayze, J. J. Wray, Orbital identification of carbonate-bearing rocks on Mars. *Science* **322**, 1828–1832 (2008).
47. J. R. Michalski, P. B. Niles, Deep crustal carbonate rocks exposed by meteor impact on Mars. *Nat. Geosci.* **3**, 751–755 (2010).
48. J. J. Wray, S. L. Murchie, J. L. Bishop, B. L. Ehlmann, R. E. Milliken, M. B. Wilhelm, K. D. Seelos, M. Chojnacki, Orbital evidence for more widespread carbonate-bearing rocks on Mars. *J. Geophys. Res. Planets* **121**, 652–677 (2016).
49. T. F. Bristow, R. M. Haberle, D. F. Blake, D. J. Des Marais, J. L. Eigenbrode, A. G. Fairén, J. P. Grotzinger, K. M. Stack, M. A. Mischna, E. B. Rampe, K. L. Siebach, B. Sutter, D. T. Vaniman, A. R. Vasavada, Low Hesperian P_{CO2} constrained from in situ mineralogical analysis at Gale Crater, Mars. *Proc. Natl. Acad. Sci. U.S.A.* **114**, 2166–2170 (2017).
50. J. A. Hurowitz, J. P. Grotzinger, W. W. Fischer, S. M. McLennan, R. E. Milliken, N. Stein, A. R. Vasavada, D. F. Blake, E. Dehouck, J. L. Eigenbrode, A. G. Fairén, J. Frydenvang, R. Gellert, J. A. Grant, S. Gupta, K. E. Herkenhoff, D. W. Ming, E. B. Rampe, M. E. Schmidt, K. L. Siebach, K. Stack-Morgan, D. Y. Sumner, R. C. Wiens, Redox stratification of an ancient lake in Gale crater, Mars. *Science* **356**, eaah6849 (2017).
51. E. B. Rampe, D. W. Ming, D. F. Blake, T. F. Bristow, S. J. Chipera, J. P. Grotzinger, R. V. Morris, S. M. Morrison, D. T. Vaniman, A. S. Yen, C. N. Achilles, P. I. Craig, D. J. Des Marais, R. T. Downs, J. D. Farmer, K. V. Fendrich, R. Gellert, R. M. Hazen, L. C. Kah, J. M. Morookian, T. S. Peretyazhko, P. Sarrazin, A. H. Treiman, J. A. Berger, J. Eigenbrode, A. G. Fairén, O. Forni, S. Gupta, J. A. Hurowitz, N. L. Lanza, M. E. Schmidt, K. Siebach, B. Sutter, L. M. Thompson, Mineralogy of an ancient lacustrine mudstone succession from the Murray formation, Gale crater, Mars. *Earth Planet. Sci. Lett.* **471**, 172–185 (2017).

Acknowledgments: We thank K. H. Miller and B. Dana, the Science Program Administrator on GSENM for permission to research the Utah nodule occurrence and for helpful advice during the field studies. We thank many people for helpful discussions, in particular Y. Sekine of the Tokyo Institute of Technology and K. Yamamoto and T. Shibata of Nagoya University. We are also grateful to S. Yogo and M. Nozaki of Nagoya University for preparing rock thin sections, SXAM mapping, and SEM-EDS analyses. We also acknowledge M. A. Chan and A. G. Fairén for detail and constructive reviews of this manuscript. **Funding:** The research was supported by JSPS KAKENHI grant 15H052227. **Author contributions:** H.Y. and H.H. designed the research and experiments and wrote the manuscript with N.K., S.S., I.M., M.M., Y.A., S.N., Y.Y., and R.M. N.K. and H.H. contributed the analysis of SXAM geochemical maps and paleoclimate analysis of Navajo Sandstone. M.M., Y.A., and R.M. carried out all other geochemical analysis and interpretation. S.N. carried out the XRD analysis of clay mineral compositions. I.M. and S.S. carried out the modeling and the bleaching experiment with carbonate and an acidic ferrous iron solution. N.I. conducted and navigated the field study in the Tugrikiin Shiree area, southern Mongolia. All authors contributed and discussed the results and provided inputs to the manuscript. **Competing interests:** The authors declare that they have no competing interests. **Data and materials availability:** All data needed to evaluate the conclusions in the paper are present in the paper and/or the Supplementary Materials. Additional data related to this paper may be requested from the corresponding authors.

Submitted 5 May 2018
Accepted 31 October 2018
Published 5 December 2018
10.1126/sciadv.aau0872

Citation: H. Yoshida, H. Hasegawa, N. Katsuta, I. Maruyama, S. Sirono, M. Minami, Y. Asahara, S. Nishimoto, Y. Yamaguchi, N. Ichinnorov, R. Metcalfe, Fe-oxide concretions formed by interacting carbonate and acidic waters on Earth and Mars. *Sci. Adv.* **4**, eaau0872 (2018).